Distribution Agreement

In presenting this thesis or dissertation as a partial fulfillment of the requirements for an advanced degree from Emory University, I hereby grant to Emory University and its agents the non-exclusive license to archive, make accessible, and display my thesis or dissertation in whole or in part in all forms of media, now or hereafter known, including display on the world wide web. I understand that I may select some access restrictions as part of the online submission of this thesis or dissertation. I retain all ownership rights to the copyright of the thesis or dissertation. I also retain the right to use in future works (such as articles or books) all or part of this thesis or dissertation.

Qiulun Li 04/10/2021

Estimating the Impact of COVID-19 on the $PM_{2.5}$ Levels in China with a Satellite-Driven Machine Learning Model

By

Qiulun Li
Master of Public Health

Gangarosa Department of Environmental Health

Yang Liu

Committee Chair

Estimating the Impact of COVID-19 on the $PM_{2.5}$ Levels in China with A Satellite-Driven Machine Learning Model

By

Qiulun Li
B.S.
Emory University
2019

Thesis Committee Chair: Yang Liu, PhD

An abstract of
A thesis submitted to the Faculty of the
Rollins School of Public Health of Emory University
in partial fulfillment of the requirements for the degree of
Master of Public Health
in Environmental Health
2021

Abstract

Estimating the Impact of COVID-19 on the $PM_{2.5}$ Levels in China with A Satellite-Driven Machine Learning Model

By Qiulun Li

China implemented an aggressive nationwide lock down procedure immediately after the COVID-19 outbreak in January 2020. As China emerges from the impact of COVID-19 on national economic and industrial activities, it became the site of a large-scale natural experiment to evaluate the impact of COVID-19 on regional air quality. However, ground measurements of $PM_{2.5}$ concentrations do not offer comprehensive spatial coverage especially in suburban and rural regions. In this study, we developed a machine learning method with satellite aerosol remote sensing data, meteorological fields and land use parameters as major predictor variables to estimate spatiotemporally resolved daily $PM_{2.5}$ concentrations in China. Our study period consists of a reference semester (November 1, 2018 – April 30, 2019) and a pandemic semester (November 1, 2019 – April 30, 2020), with six modeling months in each semester. Each period was then divided into sub-period 1 (November and December), sub-period 2 (January and February) and sub-period 3 (March and April). The reference semester model obtained a 10-fold cross-validated R^2 (RMSE) of 0.79 (17.55 $\mu g/m^3$) and the pandemic semester model obtained a 10-fold cross validated R^2 (RMSE) of 0.83 (13.48 $\mu g/m^3$) for daily $PM_{2.5}$ predictions. Our prediction results showed high $PM_{2.5}$ concentrations in the North China Plain, Yangtze River Delta, Sichuan Basin and Xinjiang Autonomous Region during the reference semester. $PM_{2.5}$ levels were lowered by 4.8 $\mu g/m^3$ during the pandemic semester comparing to the reference semester and $PM_{2.5}$ levels during sub-period 2 decreased most by 18%. The Southeast region was affected most by the COVID-19 outbreak with $PM_{2.5}$ levels during sub-period 2 decreased by 31%, following by the Northern Yangtze River Delta (29%) and Pearl River Delta (24%).

Estimating the Impact of COVID-19 on the $PM_{2.5}$ Levels in China with A Satellite-Driven Machine Learning Model

By

Qiulun Li
B.S.
Emory University
2019

Thesis Committee Chair: Yang Liu, PhD

A thesis submitted to the Faculty of the
Rollins School of Public Health of Emory University
in partial fulfillment of the requirements for the degree of
Master of Public Health
in Environmental Health
2021

Acknowledgement

I would like to thank you to my thesis advisor, Dr. Liu. Research was supported by the National Institute of Environmental Health Sciences of the National Institutes of Health (Grant No. 1R01ES032140). The content is solely the responsibility of the authors and does not necessarily represent the official views of the National Institutes of Health.

Table of Contents

1. Introduction

In December 2019, a cluster of patients infected with a novel betacoronavirus was reported in Wuhan, China [1]. The isolated virus, named SARS-CoV-2 [2], is highly infectious and rapid human-to-human transfer has been confirmed widely [1,3,4]. The coronavirus disease 2019 (COVID-19) posed global challenges for public health. As of 23 January 2020, one day before the Chinese New Year, at least 1975 cases had been reported [5] since the first hospitalized patient on 12 December. In order to contain the outbreak, China raised its national public health response to the highest state of emergency and implemented massive public health interventions. Wuhan, the epicenter of the outbreak, was the first city locked down and its neighboring cities started control thereafter. The central and local governments coordinated and implemented stringent social distancing measures and mobility restrictions [6]. The draconian interventions included isolation of suspected and confirmed cases, banning of public gatherings and close of schools as well as unnecessary commercial operations. In addition, the governments prohibited travelling in and out of cities and suspended public transport by bus and subway [7].

In addition to containing the spread of COVID-19, the lockdown and traffic restriction measures may have additional health benefits. In previous evaluations, declines of fine particulate matters ($PM_{2.5}$) and other anthropogenic air pollutants such as ozone and nitrogen dioxide had been observed. For example, from one month before and after the lockdown, Wuhan showed a decline of 36.9% in $PM_{2.5}$ levels compared with corresponding periods from 2015–2019 [8]. He et al. found similar results in which $PM_{2.5}$ levels in locked- down cities were brought down by 7.05 $\mu g/m^3$ relative to the previous year [9]. $PM_{2.5}$ is a major public health concern and its exposure has been linked to many health issues. Previous studies suggested strong positive relationships

between $PM_{2.5}$ exposure and excess mortality [10], cardiovascular disease [11–13], respiratory symptoms [14], adverse pregnancy outcomes [15,16], influenza-like illness risk [17] and others. Recent studies found that each 1 $\mu g/m^3$ increase of long-term exposure to $PM_{2.5}$ is associated with 8% increase in the COVID-19 mortality rate [18].

Accurate estimation of $PM_{2.5}$ concentrations is a prerequisite to quantify health ben- efits of reduced air pollution from COVID-19 control measures. China was a suitable study domain for air pollution research under the pandemic for two reasons. It was the first country attacked by COVID-19 epidemic and it implemented stringent countermea- sures to prevent infections. In addition, $PM_{2.5}$ is a major public health burden in China, with estimates suggesting that the air pollution contributes to 1.6 million deaths/year (0.7–2.2 million deaths/year at 95% CI), roughly 17% of the total deaths [19]. If COVID-19 control measures substantially improved the air quality in China, a greater magnitude of implied health benefits will be observed in China than in countries with lower initial air pollution levels. While many studies provided changes of $PM_{2.5}$ levels during the COVID- 19 pandemic, they used ground-based measurements [8,9,20,21]. Ground-based central $PM_{2.5}$ monitors in the regulatory network in China are unable to capture the fine scale patterns of exposure and they lack coverage in rural areas. In addition, previous studies conducted in China were at city-scale or only focused on urban areas [8,9,22,23]. There was a lack of spatiotemporally resolved $PM_{2.5}$ estimates during the COVID-19 outbreak and a comprehensive assessment of $PM_{2.5}$ levels.

In this study, we developed a machine learning model with a method, the random forest algorithm, and used a large number of datasets as predictor variables. We validated the model with 10-fold cross-validation and predicted reliable daily $PM_{2.5}$ concentrations over 5 km × 5

km grid cells across China during the study period, with a total length of 363 days. We estimated the impact of COVID-19 pandemic on $PM_{2.5}$ levels by comparing concentrations in different periods. Our spatiotemporally resolved daily $PM_{2.5}$ estimates allow epidemiologists to further quantify the health benefits of reduced air pollution with higher accuracy.

2. Materials and Methods

2.1. Study Area and Time Periods

The study domain includes mainland China, Hong Kong and Taiwan (Figure 1). It covers an area of 9.597 million km^2 and has a population of approximately 1.4 billion (http://data.stats.gov.cn/index.htm, accessed on 20 March 2021). We created a 0.05° (approximately 5 km) resolution modeling grid covering this study area for data integration, with a total of 399,513 grid cells. Our study period consists of a reference semester, from 1 November 2018 to 30 April 2019, and a pandemic semester, from 1 November 2019 to 30 April 2020. Each period was then divided into subperiod 1 (November and December), subperiod 2 (January and February) and subperiod 3 (March and April). The pandemic subperiod 2 was considered as the COVID-19 outbreak period due to high number of cases reported and the implementation of stringent control measures [6,7].

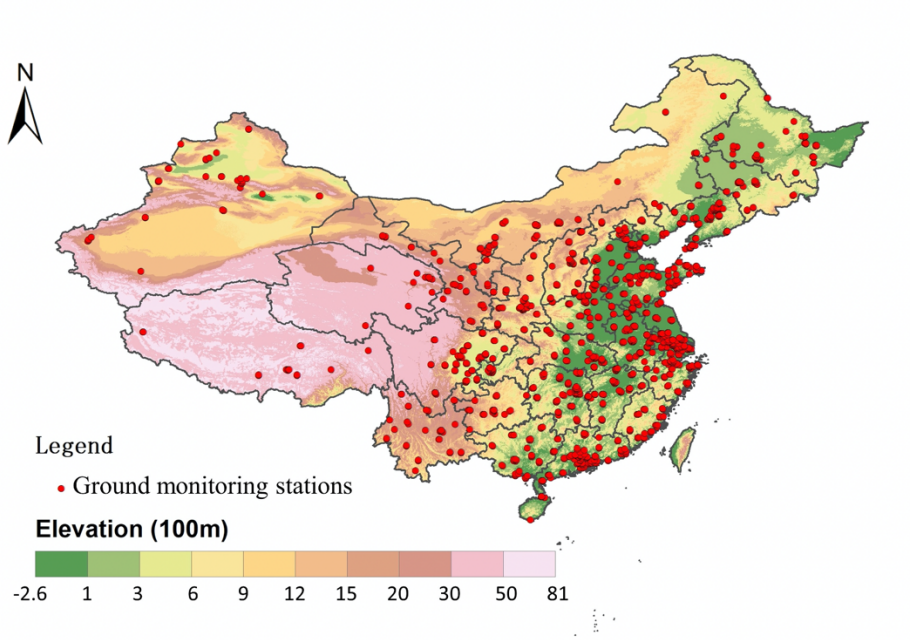

Figure 1. Map of the study domain. Ground monitoring stations are shown as red spots. China map with province outlines was downloaded from http://www. resdc.cn/, and the elevation data were obtained from the Advanced Spaceborne Thermal Emission and Reflection Radiometer (ASTER) Global Digital Elevation Model (GDEM) version 3.

2.2. Data

A summary of the datasets adopted to develop our spatial-temporal random forest models in this study is shown in Table S1 and described in detail below.

2.2.1. PM2.5 monitoring data

Hourly $PM_{2.5}$ concentrations measurements were published by the China National Environmental Monitoring Center (CNEMC, http://www.cnemc.cn) and were downloaded from PM25.in (http://pm25.in/), with 1, 534 air monitoring sites in mainland China from 2018 to 2020. We obtained $PM_{2.5}$ measurements in Hong Kong and Taiwan from the Hong Kong environmental protection department (http://epic.epd.gov.hk/) and the Taiwan environmental protection agency

(http://taqm.epa.gov.tw/), respectively. We calculated daily averaged $PM_{2.5}$ at every monitoring station and assigned monitoring stations to our modeling grid. $PM_{2.5}$ within the same grid cell were averaged, and we got as many as 1, 252 grid cells with $PM_{2.5}$ measurements.

2.2.2. MAIAC AOD data

We downloaded Terra (overpass at 10:30 am local time) and Aqua (overpass at 1:30 pm local time) multi-angle implementation of atmospheric correction (MAIAC) AOD retrievals at 0.55μm wavelength at 1 km resolution from NASA EarthData (https://search.earthdata.nasa.gov). Aerosol optical depth (AOD) is the measure of light extinction due to the presence of aerosols in the atmospheric column [24,25]. Many studies investigated the relationship between AOD and ground $PM_{2.5}$ measurements and AOD has been widely applied in $PM_{2.5}$ modeling[26,27]. MAIAC is an advanced algorithm used to retrieve daily atmospheric properties at 1 km resolution based on the measurements of the Moderate Resolution Imaging Spectroradiometer (MODIS). It used time series analysis and a combination of pixel- and image-based processing to improve accuracy of cloud detection, aerosol retrievals and atmospheric correction [28].

2.2.3. Meteorological parameters

Meteorological parameters during the study period were obtained from the Goddard Earth Observing System Data Assimilation System GEOS-5 Forward Processing (GEOS 5-FP) at a 0.25° latitude × 0.3125° longitude resolution (Lucchesi 2013). The temporal resolution was hourly for two-dimensional products and 3-hourly for three-dimensional products (Lucchesi 2013). The

meteorological data were downscaled to a 5 km grid cell by inverse distance weighting. We averaged hourly and 3-hourly GEOS 5-FP data from 10am to 4pm local time respectively to get the average weather conditions between Aqua and Terra overpass time. The full list of 15 meteorological variables used in this study can be found in the supplementary material (Table S1).

2.2.4. Land use data

We obtained the land cover data from the ESA Climate Change Initiative (CCI) global land cover at 300 m resolution (https://www.esa-landcover-cci.org). The elevation data was extracted from the Advanced Spaceborne Thermal Emission and Reflection Radiometer (ASTER) Global Digital Elevation Model (GDEM) version 3 at 30 m resolution (https://asterweb.jpl.nasa.gov/gdem.asp). In addition, we obtained the population density data from the LandScan Global population database (http://landscan.ornl.gov/) at 1km resolution.

2.3. Data integration

All predictors with various spatial resolutions were fitted into our 5-km modeling grid. The MAIAC Aqua and Terra AOD data were processed and matched to the 5-km modeling grid using nearest neighbor approach in Python (version 3.7.6). The average of Aqua and Terra measurements was calculated for daily $PM_{2.5}$ predictions. For days without Terra data, Aqua data was used to estimate the missing Terra values [29]. We multiplied Aqua values by an adjustment factor to account for diurnal variations [30]. Then we conducted aggregation or the MAIAC AOD data set by averaging multiple AOD pixels within the same modeling grid. For the meteorological fields,

the inverse distance weighting method was employed using R software (version 3.6.3). For each grid cell, the population density, elevation and land cover data were processed using ArcGIS software (version 10.7.1).

2.4. Spatial cluster analysis

Our study domain was divided into seven subregions to better characterize geographical and anthropogenic emission variations: Northeast, North, Northwest, West, Northern Yangtze River Delta (NYRD), Southeast and Pearl River Delta (PRD) (Figure 2). We fitted the same model structure in each cluster and used spatial prediction pattern for discussion. The creation of subregions followed the method of Xiao et. al.[31] but we aligned clusters more closely along provincial boundaries. The Northeast subregion consisted of three northeastern provinces, i.e., Heilongjiang, Jilin, and Liaoning, as well as eastern Inner Mongolia, where there is a long winter/heating season and large presence of heavy industry including iron and steel industry, machinery manufacturing, automobile manufacturing, oil processing, etc [32-34]. The North China Plain and the western Inner Mongolia constituted the North cluster, characterized by its coal consumption and stagnant weather, with weak wind and relatively low boundary layer height [35]. Xinjiang province constituted the Northwest cluster, characterized by substantial dust emissions from the Taklamakan Desert. Tibet plateau, Qinghai, Sichuan, Yunnan, and Gansu province constituted the West subregion with a high altitude and low population density. The Yangtze River Delta was divided into two subregions: the northern Yangtze River Delta (NYRD) with central heating in winter and the relatively warm south without central heating (Southeast). The Pearl River Delta (PRD) was another subregion, located on the coast with warm weather. The PRD and

Southeast subregions also produce more hydroelectricity than other regions. The subregion map was fitted into our 5-km modeling grid and each grid cell was assigned to a subregion.

Figure 2. Seven subregions covering the study domain and spatial distribution of $PM_{2.5}$ monitoring sites involved in this study. ArcGIS software was used for spatial cluster analysis (version 10.7.1).

2.5. $PM_{2.5}$ modeling

After integrating all datasets, we developed two separate random forest models to predict daily $PM_{2.5}$ concentrations for reference year and pandemic year, respectively. Random forest models generated rankings of variable importance, which helped us simplify the models and better understand which parameters should be refined to further improve model performance [36]. We trained the learner with ground $PM_{2.5}$ measurements as the dependent variable. Independent variables included Aqua and Terra AOD, the day of year, meteorological fields (precipitation, surface albedo, latent heat flux, surface evaporation, planetary boundary layer height, relative humidity, specific humidity, surface pressure, surface skin temperature, surface incident shortwave flux, surface velocity scale, air temperature, eastward wind component, northward wind

component) and land use parameters (population density, land cover, and elevation). Then we used trained models and predictor variables to predict daily $PM_{2.5}$ in each 5 km × 5 km grid cell. We developed two separate random forest models for reference semester and pandemic semester. Random forest models are a combination of tree predictors, and each tree is constructed using the best split for each node among a subset of predictors randomly chosen at that node [37,38]. Both models had same predictor variables while differed in their variable important rankings. By comparing the results with different settings, we set m_{try} and n_{tree} as 7 and 500 respectively to achieve the best prediction accuracy. Highly correlated variables and predictors with low importance rankings was eliminated from the model. The final $PM_{2.5}$ prediction model is expressed as:

$$PM2.5_{st} = f\ (\text{Aqua and Terra AOD}_{st}, \text{surface albedo}_{st}, \text{latent heat flux}_{st}, \text{surface evaporation}_{st}, \text{planetary boundary layer height}_{st}, \text{surface incident shortwave flux}_{st}, \text{surface velocity scale}_{st}, \text{eastward wind component}_{st}, \text{northward wind component}_{st}, \text{surface pressure}_{st}, \text{air temperature}_{st}, \text{skin temperature}_{st}, \text{precipitation}_{st}, \text{relative humidity}_{st}, \text{specific humidity}_{st}, \text{land cover}_{s}, \text{population density}_{s}, \text{elevation}_{s}).$$

where s represents the location of a grid cell and t represents the day of an observation. Variables with low importance values were discarded from the models following the variable selection strategy [37].

To assess model prediction performance, we applied 10-fold cross validation techniques. The reference year model and pandemic year model were validated separately. Each model training dataset was randomly split into 10 groups with 10% of the total data in each group. During each round of cross validation, we used nine groups to fit the random forest models and used the remaining one group as testing samples. The validation process was repeated 10 times until every

group was tested. We calculated various statistical indicators such as the coefficient of determination (R^2), mean absolute percentage error (MAPE) and root mean square error (RMSE) between cross validated predictions and observations. A comparison was conducted between the CV and model fitting statistics to test for potential model over-fitting. All statistical analyses were performed using cross_var_score, DecisionTreeRegressor and RandomForestRegressor libraries in Python software, version 3.7.6.

3. Results

3.1. Descriptive statistics

The reference semester model dataset had 181 sample days with 61 days, 59 days and 61 days in sub-periods 1, 2 and 3, respectively. The pandemic semester dataset had 182 sample days with 61 days, 60 days and 61 days in every sub-period. As shown in Table S2, the mean $PM_{2.5}$ concentrations for the reference semester was 41.30 μg/m^3 and 36.52 μg/m^3 for the pandemic semester.

During the reference year, the mean $PM_{2.5}$ concentration in sub-period 2 (45.54 μg/m^3) is noticeably higher than sub-period 1 (42.15 μg/m^3) and 3 (36.22 μg/m^3). The $PM_{2.5}$ concentrations increased during sub-period 2 probably because of the Chinese New Year migration and celebration activities such as firecracker burning [39]. In the pandemic semester model dataset, the mean $PM_{2.5}$ concentration during sub-period 2 (36.88 μg/m^3) is comparable to the other two periods (36.52 and 36.88 μg/m^3).

3.2. model performance and variable importance

The 10-fold cross-validation results for the reference semester model and pandemic semester model were presented in Figure 3. For the reference semester model, the cross-validated (CV) R^2 between fitted and observed $PM_{2.5}$ concentrations was 0.79. The MAPE and RMSE were 0.28 $\mu g/m^3$ and 17.55 $\mu g/m^3$, respectively. For the pandemic semester model, the CV R^2 increased to 0.83. The MAPE and RMSE decreased to 0.26 $\mu g/m^3$ and 13.48 $\mu g/m^3$, respectively, demonstrating a good agreement between CV predictions and ground observations. Figure 3 also showed that both models underestimated $PM_{2.5}$ concentrations at high concentration levels. The random forest algorithm presented the relative importance of predictor variable in the two prediction models by calculating %IncMSE. %IncMSE is the increase in mean square error of predictions (estimated with out-of- bag-CV) as a result of variable j being permuted (values randomly shuffled). A higher %IncMSE indicates greater importance of a variable in the prediction. For the reference semester model, the AOD parameter ranked highest in terms of importance. Meteorological parameters such as surface incident shortwave flux, planetary boundary layer height and latent heat flux, as well as the elevation also ranked high. For the pandemic semester model, the Aqua and Terra AOD and meteorological variables still ranked highest but land use parameters (population density, elevation and land cover) ranked low in terms of importance.

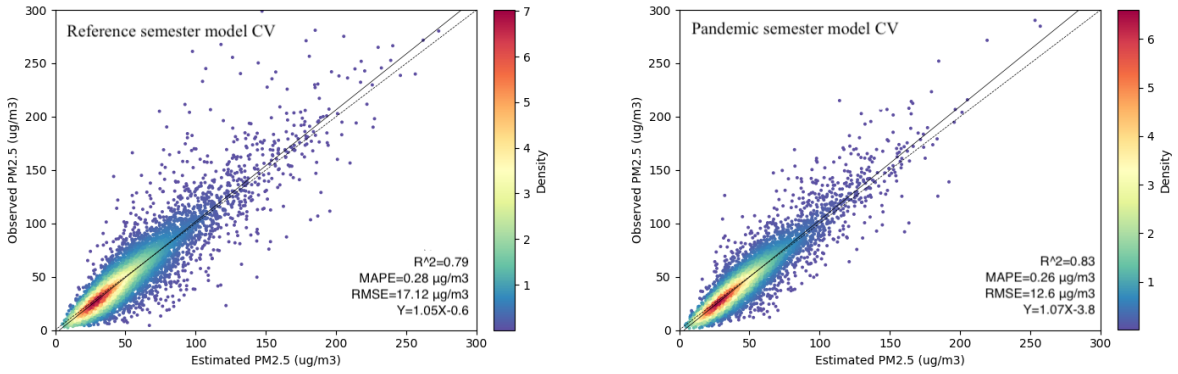

(**a**) (**b**)

Figure 3. (**a**) Density plot of ground and monitored $PM_{2.5}$ measurements in μg/m^3 based on the 10-fold cross validation of the reference semester model; (**b** Density plot of ground and monitored $PM_{2.5}$ measurements in μg/m^3 based on the 10-fold cross validation of the pandemic semester model.

3.3. $PM_{2.5}$ predictions

The spatial distribution of mean $PM_{2.5}$ predictions during sub-period 1, 2 and 3 by the reference semester model and pandemic semester model was presented in Figure 4. The reference semester model had a spatial coverage of 95% for sub-period 1, 87% for sub-period 2, and 96% for sub-period 3. The mean $PM_{2.5}$ concentrations in every sub-period (1, 2 and 3) were 41.25 μg/m^3, 45.54 μg/m^3 and 36.22 μg/m^3, respectively. For the reference semester model, maps showed similar spatial patterns of $PM_{2.5}$ concentrations in sub-period 1 and 2. The mean $PM_{2.5}$ distribution maps during these two periods (Figure 4A and B) showed regions with elevated $PM_{2.5}$ levels in the North China Plain, including Beijing, Tianjin, Hebei province and Henan province, as well as the NYRD region. The NYRD region had highest $PM_{2.5}$ concentrations during sub-period 1 and 2 - 68.72 μg/m^3 and 74.35 μg/m^3, respectively, comparing to other regions (Table 1). The rapid urbanization, high population density and local economic growth were main driving forces of high $PM_{2.5}$ concentrations in East China [40,41]. There were also some hotspots in the Sichuan Basin, especially in two megacities – Chengdu and Chongqing [42]. The Sichuan Bason is completely encircled by high mountains and plateaus. It is also characterized by persistently high relative humidity as well as low wind speeds [43,44]. The discharge of anthropogenic pollutants in combination with the special topography and meteorological conditions limits the diffusion of pollutants in this region [42,45,46]. In addition, high levels of $PM_{2.5}$ pollution was found in the northwestern region, especially in the southern Xinjiang Autonomous Region where the Taklamakan Desert covered 60% of this region. The mean $PM_{2.5}$ concentrations during sub-

period 1 and 2 in the northwestern region was 57.45 μg/m^3 and 60.66 μg/m^3, respectively. The accumulation of dust particles in the winter contributed to the high level of $PM_{2.5}$ pollution in this region [35,47]. During sub-period 3 (Figure 4C), $PM_{2.5}$ concentrations stayed high in the northwestern region (56.29 μg/m^3) but substantially decreased in the NYRD region (44.58 μg/m^3).

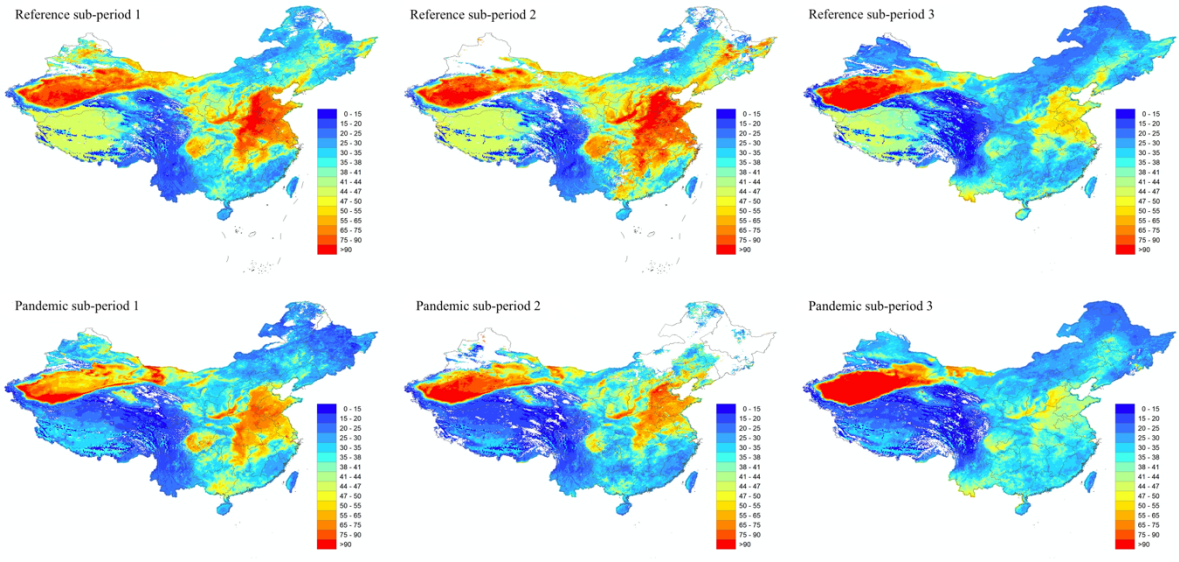

Figure 4. Average $PM_{2.5}$ distribution in the reference semester (above) and pandemic semester (below). ArcGIS was used to visualize the spatial distribution (version 10.7.1).

For the pandemic semester model, the spatial coverage for mean $PM_{2.5}$ concentrations during sub-period 1, 2 and 3 were 96%, 79% and 96%, respectively. The mean $PM_{2.5}$ distribution map for sub-period 1 (Figure 4D) indicated high $PM_{2.5}$ concentrations in the North China Plain, Yangtze River Delta, Sichuan Basin and northwestern region. During sub-period 2 and 3 (Figure 4E and F), there were fewer hotspots in eastern China and Sichuan Basin while $PM_{2.5}$ concentrations significantly increased in the northwestern region. Then mean $PM_{2.5}$ concentrations in the Northwestern region in each sub-period (1, 2 and 3) were 46.74 μg/m^3, 54.18 μg/m^3 and 68.67 μg/m^3, respectively.

Table 1. Summary statistics of $PM_{2.5}$ predictions by cluster during modeling periods (μg/m^3).

	Period 1	Period 2	Period 3
Reference semester			
North	47.10	52.41	33.69
Northwest	57.45	60.66	56.29
Northeast	33.65	37.67	28.67
Qinghai-Tibet	33.55	33.97	30.25
NYRD	68.72	74.35	44.58
Southeast	35.23	45.25	31.84
PRD	36.55	46.46	33.39
Pandemic semester			
North	40.46	44.53	35.20
Northwest	46.72	54.18	68.67
Northeast	26.73	37.77	27.92
Qinghai-Tibet	27.39	24.76	26.08
NYRD	57.52	51.80	39.48
Southeast	35.45	29.46	32.38
PRD	41.20	32.84	34.51

4. Discussion

Our machine learning method had strong potentials to estimate $PM_{2.5}$ concentrations and presented spatial and temporal variability during the COVID-19 outbreak. Our model demonstrated high prediction accuracy on a national scale and yielded a similar CV R^2 to previous studies conducted in China [31,46]. Additionally, our study domain is geographically board, which allowed us to explore spatial variations across China. Many studies examining changes in $PM_{2.5}$ pollution during the pandemic relied solely on ground measurements, which failed to provide comprehensive spatial coverage especially in suburban and rural regions. As a result, previous studies could only focus on certain cities or one city-cluster region [8,23].

Our reference semester model showed high $PM_{2.5}$ concentrations in the North China Plain, northern Yangtze River Delta, Sichuan Basin and Xinjiang Autonomous Region. Overall, the levels of $PM_{2.5}$ pollution were higher in the northern regions than in the southern regions. Our

predictions showed similar spatial distributions and variations compared with other studies in these regions [27,46,48-51]. The intensive human activities (i.e. industrial activities, fossil fuel combustion and agricultural waste burning) and unfavorable meteorological conditions (low boundary layer height and weak wind) led to high $PM_{2.5}$ concentrations in the North China Plain [41,46,51]. The main reasons for the serious $PM_{2.5}$ pollution in the Yangtze River Delta were high population density and rapid urbanization [40]. The Sichuan Basin had high $PM_{2.5}$ pollution due to its unique topography. Persistent temperature inversion and stagnant air circulation always occurred in this region [51]. Additionally, the dust storms in the desert region led to serious $PM_{2.5}$ pollution in Xinjiang Autonomous Region [47]. Low $PM_{2.5}$ pollution occurred in the northeastern region characterized by its dense vegetation cover. The southern region generally had low $PM_{2.5}$ concentrations benefiting from its favorable meteorological conditions (i.e. high precipitation and southerly flow) for atmospheric dispersion [52].

Our model predictions allowed us to explore the impact of COVID-19 on $PM_{2.5}$ levels during the pandemic semester. $PM_{2.5}$ levels were lowered by 4.8 $\mu g/m^3$ during the pandemic semester as compared to the reference semester. We also calculated the relative difference between the reference semester model and semester year model predictions. Comparing with the reference semester, $PM_{2.5}$ levels in pandemic sub-period 1 and 2 decreased by 13% and 18% but increased slightly by 0.48% in sub-period 3 (Figure 5). During the pandemic sub-period 1, the COVID-19 transmissibility had not been confirmed and no control measure had been implemented. $PM_{2.5}$ concentrations decreased most in Northeast, Northwest and Qinghai-Tibet regions by 18%, 17% and 15%, respectively (Table 2). The decrease of $PM_{2.5}$ levels in these regions of low population density was likely due to favorable meteorological conditions. China meteorological administration observed a significant increase in precipitation in Tibet and denser vegetation cover

in the Northeast region (http://www.cma.gov.cn). The increased green space was able to regulate microclimatic conditions and reduce pollutants through filtration [53-55]. During sub-period 2, a significantly greater reduction in $PM_{2.5}$ levels (18%, $p<0.05$) was observed due to the COVID-19 outbreak, when lockdown and stringent traffic restrictions were implemented by the governments. $PM_{2.5}$ levels in the Southeast region decreased most by 31%, followed by NYRD (29%) and PRD (24%). Yangtze River Delta and Pearl River Delta were major economic city-clusters in China. As they entered Level I public health response period (January 24 – February 25), cities reduced the number of people and vehicles in public places and closed all industrial enterprises, construction sites and recreational operations [22]. Other studies focused on these two regions showed similar results. Li et al. (2020) found concentrations of $PM_{2.5}$ decreased by 31.8% during the Level I period in the NYRD Region compared with 2019 [22]. He et al. (2020) confirmed a reduction in the AQI around 5-10 points, converted to a reduction in $PM_{2.5}$ around 1.2-2.4 $\mu g/m^3$, in the Southern China during the lockdown period relative to the previous year [9]. During this period, hotspots of $PM_{2.5}$ were observed in Beijing-Tianjin-Hebei Region. The increase of $PM_{2.5}$ levels in this region was contrary to the overall decreasing trend in the North Region by 12%. Other studies that conducted atmospheric and transport model simulations in Beijing-Tianjin-Hebei region showed similar $PM_{2.5}$ concentration patterns during this period. Le et al. (2020) observed severe haze events in Beijing during the outbreak period and increased mean surface $PM_{2.5}$ by 55.1% comparing to the same period of 2015 to 2019 [56]. Unfavorable meteorological conditions such as low wind speed and high relative humidity in BTH Region might explain increased $PM_{2.5}$ levels [56-58]. During pandemic sub-period 3, cities with low risk of COVID-19 infection started to reopen and most activities entered into operation. Comparing with the pandemic year period 2, $PM_{2.5}$ levels statistically increased in the Southeast, Northwest, PRD, NYRD and North regions. $PM_{2.5}$

concentrations increased in the Northwest region due to frequent dust storms occurring in spring in the desert, semi-desert and grassland areas [59]. The temporal variability in other regions could be explained by increased human activities and industrial emissions in Yangtze River Delta, Pearl River Delta and North China Plain after the reopen. During this period, citizens were allowed to travel locally with health code and protection measures; commercial and industrial enterprises were allowed to resume work.

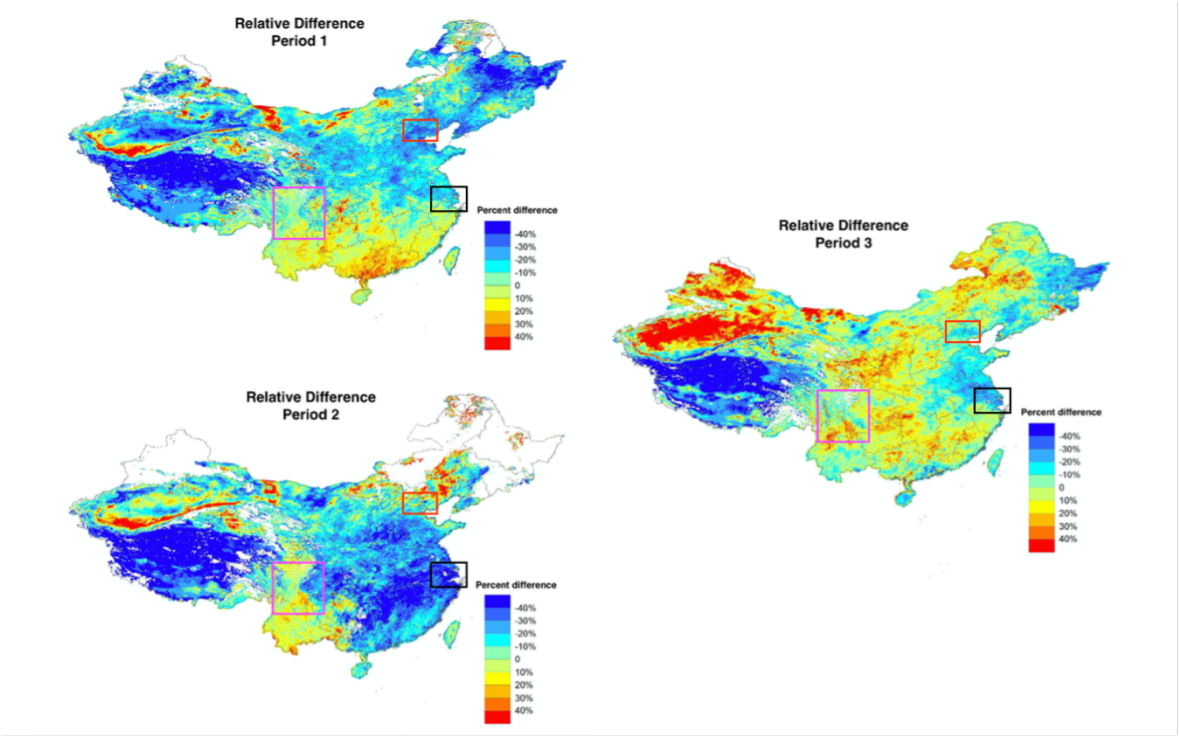

Figure 5. Estimated $PM_{2.5}$ change rates between the reference semester model and pandemic semester model predictions. Beijing-Tianjin-Hebei region, Yangtze River Delta and Sichuan Basin were marked in red, black and purple, respectively.

We were able to compare changes of $PM_{2.5}$ levels in different land cover types. As we observed an overall decline of $PM_{2.5}$ concentrations, urban areas had a larger reduction than in rural areas during the COVID-19 outbreak (Table 2). Several reasons could explain this disparity. First, the mass human migration during the Spring Festival travel led to the change of population distribution patterns in China. There was a significant reduction in population density in urban

areas during the holiday period [60]. Combing with the COVID-19 control measures, the greater reduction in human activities in urban areas contributed to greater decrease in $PM_{2.5}$ levels. Secondly, the proportion of bulk coal heating users increased in the rural areas due to the return of migrant workers and the lack of central heating. The increasing emissions may have mitigated reductions resulted from COVID-19 control measures. Moreover, life-essential industrial facilities such as power plants are located in rural areas and stayed operating during the COVID-19 outbreak, while other industrial facilities and entertainment operations were closed in urban areas.

One limitation of this study is the incomplete spatial coverage due to cloud and snow cover, especially in northeastern China, which may introduce region-specific sampling biases when estimating mean $PM_{2.5}$ levels in each period. We will address this issue in the future with a gap-filling method. Overall, we have a high spatial coverage and these missing values will not significantly alter our results. Another limitation of this study is the uneven distribution of ground monitoring measurements across the study domain. There are fewer monitor locations in the Northwest and Qinghai-Tibet comparing to other regions. Although our models reached high prediction accuracy, the lack of ground measurements for model training possibly influences the model performance in these two regions. We will address this issue in the future research by fitting separate models in every cluster.

Table 2. Estimated $PM_{2.5}$ change rates by region and by land type during modeling periods (%).

Region	Period 1	Period 2	Period 3
North	-12.77	-12.68	5.45
Northwest	-16.91	-9.03	20.25
Northeast	-18.42	7.03	-0.16
Qinghai-Tibet	-15.24	-21.5	-10.08
NYRD	-14.56	-29.39	-9.48
Southeast	2.63	-31.05	3.14
PRD	13.92	-23.8	5.35
Urban	-13.49	-25.12	-7.33
Rural	-9.78	-19.68	1.22

5. Conclusions

We developed a machine learning method with satellite-derived data as major predictor variables to provide spatiotemporally resolved daily $PM_{2.5}$ estimates (reference semester model: CV $R^2 = 0.79$, and pandemic semester model: CV $R^2 = 0.83$). Our results showed that the $PM_{2.5}$ levels were lowered by 4.8 μg/m3 during the pandemic semester comparing to the reference semester. COVID-19 control measures implemented during sub-period 2 caused significant reduction in $PM_{2.5}$ levels by 18%. The Southeast region decreased most by 31% and the urban areas decreased more than rural areas. Though $PM_{2.5}$ concentrations dropped significantly during the COVID-19 lockdown, the national average was still three times higher than safety levels suggested by the World Health Organization (10 $\mu g/m^3$ for the annual mean). Our paper is useful for future research to understand the full implications from this unprecedented event and is informative for more stringent air pollution regulations. Our $PM_{2.5}$ predictions can be used to calculate the decreased disease burden resulted from $PM_{2.5}$ pollution during COVID-19 pandemic.

6. References

1. Zhu, N.; Zhang, D.; Wang, W.; Li, X.; Yang, B.; Song, J.; Zhao, X.; Huang, B.; Shi, W.; Lu, R. A novel coronavirus from patients with pneumonia in China, 2019. *New England Journal of Medicine* **2020**, doi:10.1056/NEJMoa2001017.
2. Yuen, K.-S.; Ye, Z.-W.; Fung, S.-Y.; Chan, C.-P.; Jin, D.-Y. SARS-CoV-2 and COVID-19: The most important research questions. *Cell Biosci* **2020**, *10*, 40-40, doi:10.1186/s13578-020-00404-4.
3. Zhou, P.; Yang, X.-L.; Wang, X.-G.; Hu, B.; Zhang, L.; Zhang, W.; Si, H.-R.; Zhu, Y.; Li, B.; Huang, C.-L. A pneumonia outbreak associated with a new coronavirus of probable bat origin. *nature* **2020**, *579*, 270-273, doi:10.1038/s41586-020-2012-7.
4. Shereen, M.A.; Khan, S.; Kazmi, A.; Bashir, N.; Siddique, R. COVID-19 infection: Origin, transmission, and characteristics of human coronaviruses. *Journal of Advanced Research* **2020**, doi:10.1016/j.jare.2020.03.005.
5. Wu, F.; Zhao, S.; Yu, B.; Chen, Y.-M.; Wang, W.; Song, Z.-G.; Hu, Y.; Tao, Z.-W.; Tian, J.-H.; Pei, Y.-Y. A new coronavirus associated with human respiratory disease in China. *Nature* **2020**, *579*, 265-269, doi:10.1038/s41586-020-2008-3.

6. Leung, K.; Wu, J.T.; Liu, D.; Leung, G.M. First-wave COVID-19 transmissibility and severity in China outside Hubei after control measures, and second-wave scenario planning: a modelling impact assessment. *The Lancet* **2020**, doi:10.1016/s0140-6736(20)30746-7.
7. Tian, H.; Liu, Y.; Li, Y.; Wu, C.-H.; Chen, B.; Kraemer, M.U.; Li, B.; Cai, J.; Xu, B.; Yang, Q. An investigation of transmission control measures during the first 50 days of the COVID-19 epidemic in China. *Science* **2020**, *368*, 638-642, doi:10.1126/science.abb6105.
8. Lian, X.; Huang, J.; Huang, R.; Liu, C.; Wang, L.; Zhang, T. Impact of city lockdown on the air quality of COVID-19-hit of Wuhan city. *Science of the Total Environment* **2020**, *742*, 140556, doi:10.1016/jscitoten.2020.140556.
9. He, G.; Pan, Y.; Tanaka, T. The short-term impacts of COVID-19 lockdown on urban air pollution in China. *Nature Sustainability* **2020**, 1-7, doi:10.1038/s41893-020-0581-y.
10. Di, Q.; Wang, Y.; Zanobetti, A.; Wang, Y.; Koutrakis, P.; Choirat, C.; Dominici, F.; Schwartz, J.D. Air pollution and mortality in the Medicare population. *New England Journal of Medicine* **2017**, *376*, 2513-2522, doi:10.1056/NEJMoa1702747.
11. Haikerwal, A.; Akram, M.; Del Monaco, A.; Smith, K.; Sim, M.R.; Meyer, M.; Tonkin, A.M.; Abramson, M.J.; Dennekamp, M. Impact of fine particulate matter (PM 2.5) exposure during wildfires on cardiovascular health outcomes. *Journal of the American Heart Association* **2015**, *4*, e001653, doi:10.1161/JAHA.114.001653.
12. Lee, B.-J.; Kim, B.; Lee, K. Air pollution exposure and cardiovascular disease. *Toxicological research* **2014**, *30*, 71-75, doi:10.5487/TR.2014.30.2.071.
13. Pope III, C.A.; Burnett, R.T.; Thurston, G.D.; Thun, M.J.; Calle, E.E.; Krewski, D.; Godleski, J.J. Cardiovascular mortality and long-term exposure to particulate air pollution: epidemiological evidence of general pathophysiological pathways of disease. *Circulation* **2004**, *109*, 71-77, doi:10.1161/01.CIR.0000108927.80044.7F.
14. Dominici, F.; Peng, R.D.; Bell, M.L.; Pham, L.; McDermott, A.; Zeger, S.L.; Samet, J.M. Fine particulate air pollution and hospital admission for cardiovascular and respiratory diseases. *Jama* **2006**, *295*, 1127-1134, doi:10.1001/jama.295.10.1127.
15. Kloog, I.; Melly, S.J.; Ridgway, W.L.; Coull, B.A.; Schwartz, J. Using new satellite based exposure methods to study the association between pregnancy PM 2.5 exposure, premature birth and birth weight in Massachusetts. *Environmental Health* **2012**, *11*, 1-8, doi:10.1186/1476-069X-11-40.
16. Zhu, X.; Liu, Y.; Chen, Y.; Yao, C.; Che, Z.; Cao, J. Maternal exposure to fine particulate matter (PM 2.5) and pregnancy outcomes: a meta-analysis. *Environmental Science and Pollution Research* **2015**, *22*, 3383-3396, doi:10.1007/s11356-014-3458-7.
17. Feng, C.; Li, J.; Sun, W.; Zhang, Y.; Wang, Q. Impact of ambient fine particulate matter (PM 2.5) exposure on the risk of influenza-like-illness: a time-series analysis in Beijing, China. *Environmental Health* **2016**, *15*, 17, doi:10.1186/s12940-016-0115-2.
18. Wu, X.; Nethery, R.C.; Sabath, B.M.; Braun, D.; Dominici, F. Exposure to air pollution and COVID-19 mortality in the United States. *medRxiv* **2020**, doi:10.1126/sciadv.abd4049.
19. Liang, F.; Xiao, Q.; Huang, K.; Yang, X.; Liu, F.; Li, J.; Lu, X.; Liu, Y.; Gu, D. The 17-y spatiotemporal trend of PM_{2.5} and its mortality burden in China. *Proceedings of the National Academy of Sciences* **2020**, *117*, 25601, doi:10.1073/pnas.1919641117.

20. Berman, J.D.; Ebisu, K. Changes in US air pollution during the COVID-19 pandemic. *Science of the Total Environment* **2020**, *739*, 139864.
21. Zangari, S.; Hill, D.T.; Charette, A.T.; Mirowsky, J.E. Air quality changes in New York City during the COVID-19 pandemic. *Science of the Total Environment* **2020**, *742*, 140496, doi:10.1016/j.scitotenv.2020.140496.
22. Li, L.; Li, Q.; Huang, L.; Wang, Q.; Zhu, A.; Xu, J.; Liu, Z.; Li, H.; Shi, L.; Li, R. Air quality changes during the COVID-19 lockdown over the Yangtze River Delta Region: An insight into the impact of human activity pattern changes on air pollution variation. *Science of The Total Environment* **2020**, 139282, doi:10.1016/j.scitotenv.2020.139282.
23. He, G.; Pan, Y.; Tanaka, T. COVID-19, City Lockdowns, and Air Pollution: Evidence from China. *medRxiv* **2020**, doi:10.1038/s41893-020-0581-y.
24. Donkelaar, A.v.; Martin, R.V.; Brauer, M.; Kahn, R.; Levy, R.; Verduzco, C.; Villeneuve, P.J. Global Estimates of Ambient Fine Particulate Matter Concentrations from Satellite-Based Aerosol Optical Depth: Development and Application. *Environ Health Perspect* **2010**, *118*, 847-855, doi:10.1289/ehp.0901623.
25. Chudnovsky, A.A.; Koutrakis, P.; Kloog, I.; Melly, S.; Nordio, F.; Lyapustin, A.; Wang, Y.; Schwartz, J. Fine particulate matter predictions using high resolution Aerosol Optical Depth (AOD) retrievals. *Atmospheric Environment* **2014**, *89*, 189-198, doi:10.1016/j.atmosenv.2014.02.019.
26. Hu, X.; Waller, L.A.; Lyapustin, A.; Wang, Y.; Al-Hamdan, M.Z.; Crosson, W.L.; Estes, M.G.; Estes, S.M.; Quattrochi, D.A.; Puttaswamy, S.J. Estimating ground-level PM2.5 concentrations in the Southeastern United States using MAIAC AOD retrievals and a two-stage model. *Remote. Sens. Environ.* **2014**, *140*, 220, doi:10.1016/j.rse.2013.08.032.
27. Ma, Z.; Hu, X.; Sayer, A.M.; Levy, R.; Zhang, Q.; Xue, Y.; Tong, S.; Bi, J.; Huang, L.; Liu, Y. Satellite-Based Spatiotemporal Trends in PM2.5 Concentrations: China, 2004-2013. *Environ Health Perspect* **2016**, *124*, 184-192, doi:10.1289/ehp.1409481.
28. Lyapustin, A.; Wang, Y.; Korkin, S.; Huang, D. MODIS Collection 6 MAIAC algorithm. *Atmospheric Measurement Techniques* **2018**, *11*, 5741-5765, doi:10.5194/amt-11-5741-2018.
29. Green, M.; Kondragunta, S.; Ciren, P.; Xu, C. Comparison of GOES and MODIS aerosol optical depth (AOD) to aerosol robotic network (AERONET) AOD and IMPROVE PM2. 5 mass at Bondville, Illinois. *Journal of the Air & Waste Management Association* **2009**, *59*, 1082-1091, doi:10.3155/1047-3289.59.9.1082.
30. Puttaswamy, S.J.; Nguyen, H.M.; Braverman, A.; Hu, X.; Liu, Y. Statistical data fusion of multi-sensor AOD over the Continental United States. *Geocarto Int.* **2013**, 1, doi:10.1080/10106049.2013.827750.
31. Xiao, Q.; Chang, H.H.; Geng, G.; Liu, Y. An ensemble machine-learning model to predict historical PM2. 5 concentrations in China from satellite data. *Environmental science & technology* **2018**, *52*, 13260-13269, doi:10.1021/acs.est.8b02917.
32. Song, N.; Ma, J.; Yu, Y.; Yang, Z.; Li, Y. New observations on PAH pollution in old heavy industry cities in northeastern China. *Environmental Pollution* **2015**, *205*, 415-423, doi:10.1016/j.envpol.2015.07.005.
33. Kong, S.; Shi, J.; Lu, B.; Qiu, W.; Zhang, B.; Peng, Y.; Zhang, B.; Bai, Z. Characterization of PAHs within PM10 fraction for ashes from coke production, iron smelt, heating station and power plant stacks in Liaoning Province, China. *Atmospheric Environment* **2011**, *45*, 3777-3785, doi:10.1016/j.atmosenv.2011.04.029.

34. Sun, L.; Zang, S.Y.; Sun, H.J. Sources and history of PAHs in lake sediments from oil-producing and industrial areas, northeast China. *International Journal of Environmental Science and Technology* **2014**, *11*, 2051-2060, doi:10.1007/s13762-013-0396-8, doi:10.1007/s13762-013-0396-8.
35. Chen, Z.; Cheng, S.; Li, J.; Guo, X.; Wang, W.; Chen, D. Relationship between atmospheric pollution processes and synoptic pressure patterns in northern China. *Atmospheric Environment* **2008**, *42*, 6078-6087, doi:10.1016/j.atmosenv.2008.03.043.
36. Huang, K.; Bi, J.; Meng, X.; Geng, G.; Lyapustin, A.; Lane, K.J.; Gu, D.; Kinney, P.L.; Liu, Y. Estimating daily PM2. 5 concentrations in New York City at the neighborhood-scale: Implications for integrating non-regulatory measurements. *Science of The Total Environment* **2019**, *697*, 134094, doi:10.1016/j.scitotenv.2019.134094.
37. Hu, X.; Belle, J.H.; Meng, X.; Wildani, A.; Waller, L.A.; Strickland, M.J.; Liu, Y. Estimating PM2. 5 concentrations in the conterminous United States using the random forest approach. *Environmental science & technology* **2017**, *51*, 6936-6944, doi:10.1021/acs.est.7b01210.
38. Breiman, L. Random Forests. *Machine Learning* **2001**, *45*, 5-32, doi:10.1023/A:1010933404324.
39. Ye, C.; Chen, R.; Chen, M. The impacts of Chinese Nian culture on air pollution. *Journal of Cleaner Production* **2016**, *112*, 1740-1745, doi:10.1016/j.jclepro.2015.04.113.
40. Lin, G.; Fu, J.; Jiang, D.; Hu, W.; Dong, D.; Huang, Y.; Zhao, M. Spatio-temporal variation of PM2. 5 concentrations and their relationship with geographic and socioeconomic factors in China. *International journal of environmental research and public health* **2014**, *11*, 173-186, doi:10.3390/ijerph110100173.
41. Li, T.; Shen, H.; Zeng, C.; Yuan, Q.; Zhang, L. Point-surface fusion of station measurements and satellite observations for mapping PM2. 5 distribution in China: Methods and assessment. *Atmospheric Environment* **2017**, *152*, 477-489, doi:10.1016/j.atmosenv.2017.01.004.
42. Wang, H.; Tian, M.; Chen, Y.; Shi, G.; Liu, Y.; Yang, F.; Zhang, L.; Deng, L.; Yu, J.; Chao, P. Seasonal characteristics, formation mechanisms and source origins of PM 2.5 in two megacities in Sichuan Basin, China. *Atmospheric Chemistry and Physics* **2018**, *18*, 865, doi:10.5194/acp-18-865-2018.
43. Guo, M.; Cai, X.; Song, Y. Characteristics of low wind-speed meteorology in China. **2016**, *52*, 219-226, doi:10.13209/j.0479-8023.2015.116.
44. Chen, Y.; Xie, S.-d. Long-term trends and characteristics of visibility in two megacities in southwest China: Chengdu and Chongqing. *Journal of the Air & Waste Management Association* **2013**, *63*, 1058-1069, doi:10.1080/10962247.2013.791348.
45. Wang, X.; Dickinson, R.E.; Su, L.; Zhou, C.; Wang, K. PM2. 5 pollution in China and how it has been exacerbated by terrain and meteorological conditions. *Bulletin of the American Meteorological Society* **2018**, *99*, 105-119, doi:10.1175/BAMS-D-16-0301.1.
46. Wei, J.; Huang, W.; Li, Z.; Xue, W.; Peng, Y.; Sun, L.; Cribb, M. Estimating 1-km-resolution PM2. 5 concentrations across China using the space-time random forest approach. *Remote Sensing of Environment* **2019**, *231*, 111221, doi:10.1016/j.rse.2019.111221.
47. Fang, X.; Zou, B.; Liu, X.; Sternberg, T.; Zhai, L. Satellite-based ground PM2. 5 estimation using timely structure adaptive modeling. *Remote Sensing of Environment* **2016**, *186*, 152-163, doi:10.1016/j.rse.2016.08.027.

48. Ma, Z.; Hu, X.; Huang, L.; Bi, J.; Liu, Y. Estimating Ground-Level PM2.5 in China Using Satellite Remote Sensing. *Environmental Science & Technology* **2014**, *48*, 7436-7444, doi:10.1021/es5009399.
49. He, Q.; Huang, B. Satellite-based mapping of daily high-resolution ground PM2.5 in China via space-time regression modeling. *Remote Sensing of Environment* **2018**, *206*, 72-83, doi:10.1016/j.rse.2017.12.018.
50. Zhang, M.; Wang, X.; Chen, J.; Cheng, T.; Wang, T.; Yang, X.; Gong, Y.; Geng, F.; Chen, C. Physical characterization of aerosol particles during the Chinese New Year's firework events. *Atmospheric Environment* **2010**, *44*, 5191-5198, doi:10.1016/j.atmosenv.2010.08.048.
51. You, W.; Zang, Z.; Zhang, L.; Li, Y.; Pan, X.; Wang, W. National-Scale Estimates of Ground-Level PM2.5 Concentration in China Using Geographically Weighted Regression Based on 3 km Resolution MODIS AOD. *Remote Sensing* **2016**, *8*, 184, doi:10.3390/rs8030184.
52. Zhai, S.; Jacob, D.J.; Wang, X.; Shen, L.; Li, K.; Zhang, Y.; Gui, K.; Zhao, T.; Liao, H. Fine particulate matter (PM2.5) trends in China, 2013–2018: separating contributions from anthropogenic emissions and meteorology. *Atmos. Chem. Phys.* **2019**, *19*, 11031-11041, doi:10.5194/acp-19-11031-2019.
53. Hwang, H.-J.; Yook, S.-J.; Ahn, K.-H. Experimental investigation of submicron and ultrafine soot particle removal by tree leaves. *Atmospheric Environment* **2011**, *45*, 6987-6994, doi:10.1016/j.atmosenv.2011.09.019.
54. Lafortezza, R.; Carrus, G.; Sanesi, G.; Davies, C. Benefits and well-being perceived by people visiting green spaces in periods of heat stress. *Urban Forestry & Urban Greening* **2009**, *8*, 97-108, doi:10.1016/j.ufug.2009.02.003.
55. Chen, J.; Zhu, L.; Fan, P.; Tian, L.; Lafortezza, R. Do green spaces affect the spatiotemporal changes of PM2.5 in Nanjing? *Ecological Processes* **2016**, *5*, 7, doi:10.1186/s13717-016-0052-6.
56. Le, T.; Wang, Y.; Liu, L.; Yang, J.; Yung, Y.L.; Li, G.; Seinfeld, J.H. Unexpected air pollution with marked emission reductions during the COVID-19 outbreak in China. *Science* **2020**, *369*, 702-706, doi:10.1126/science.abb7431.
57. Zhao, N.; Wang, G.; Li, G.; Lang, J.; Zhang, H. Air pollution episodes during the COVID-19 outbreak in the Beijing–Tianjin–Hebei region of China: An insight into the transport pathways and source distribution. *Environmental Pollution* **2020**, *267*, 115617, doi:10.1016/j.envpol.2020.115617.
58. Wang, P.; Chen, K.; Zhu, S.; Wang, P.; Zhang, H. Severe air pollution events not avoided by reduced anthropogenic activities during COVID-19 outbreak. *Resources, Conservation and Recycling* **2020**, *158*, 104814, doi:10.1016/j.resconrec.2020.104814.
59. Zou, X.K.; Zhai, P.M. Relationship between vegetation coverage and spring dust storms over northern China. *Journal of Geophysical Research: Atmospheres* **2004**, *109*, doi:10.1029/2003jd003913.
60. Hu, M. Visualizing the largest annual human migration during the Spring Festival travel season in China. *Environment and Planning A: Economy and Space* **2019**, *51*, 1618-1621, doi:10.1177/0308518x19845908.

7. Supplementary Materials

Table S1. Summary statistics of $PM_{2.5}$ predictions by cluster during modeling periods ($\mu g/m^3$).

Source category	Data source	Variables	Resolution	
			Spatial	Temporal
$PM_{2.5}$	CNEMC	$PM_{2.5}$	Monitoring stations	hourly
	Hongkong EPD	$PM_{2.5}$	Monitoring stations	hourly
	Taiwan EPA	$PM_{2.5}$	Monitoring stations	hourly
AOD	MAIAC	Aqua and Terra AOD	1 km	daily
Meteorology	GEOS 5-FP	precipitation, surface albedo, latent heat flux, surface evaporation, planetary boundary layer height, relative humidity, specific humidity, surface pressure, surface skin temperature, surface incident shortwave flux, surface velocity scale, air temperature, eastward wind component, northward wind component	0.25° latitude × 0.3125° longitude	Hourly and 3-hourly
Land cover	ESA CCI	types of land cover	300 m	none
Population	LandScan	population density	1 km	none
Elevation	ASTER	Global Digital Elevation Model (GDEM) version 3	30 m	none

Table S2. summary statistics of $PM_{2.5}$ predictions, satellite AOD and major meteorological observations during modeling periods.

	Overall Mean	Period 1 (11/01 - 12/31)				Period 2 (1/01 - 2-28)				Period 3 (3/01 - 4/30)			
		Mean	SD	Max	Min	Mean	SD	Max	Min	Mean	SD	Max	Min
Reference year		N = 61				N = 59				N = 61			
PM2.5 ($\mu g/m^3$)	41.30	42.15	19.26	199	9.22	45.54	21.61	261	6.61	36.22	20.44	293	6.68
Aqua and Terra AOD	0.2	0.16935	0.21	3.92	0.002	0.19	0.25	3.92	0.003	0.25	0.36	3.92	0.003
Albedo	0.25	0.25	0.12	0.83	0.064	0.28	0.14	0.85	0.063	0.23	0.12	0.84	0.057
EFLUX	68	54	56	1426	-26	50	50	1248	-7.21	101	86	910	-55
QV2M	3.281×10^{-3}	3.018×10^{-3}	2.89×10^{-3}	1.87×10^{-2}	9.89×10^{-5}	2.53×10^{-3}	2.36×10^{-3}	1.78×10^{-2}	9.04×10^{-5}	4.3×10^{-3}	3.75×10^{-3}	2.21×10^{-2}	2.73×10^{-4}
PBLH	1121	890	544	3690	55	933	637	3917	54	1540	711	4561	57
SWGDN	457	362	150	758	3.81	397	157	839	7.62	613	190	1041	26.09
RH	0.46	0.45	0.21	1	0.0098	0.52	0.21	1	0.15	0.41	0.22	1	0.031
Pandemic year		N = 61				N = 60				N = 61			
PM2.5 ($\mu g/m^3$)	36.52	35.81	17.62	317	4.42	36.88	20.10	342	4.57	36.88	28.54	352	4.20
Aqua and Terra AOD	0.23	0.18	0.21	3.92	0	0.21	0.27	3.92	0.005	0.3	0.42	3.92	0.004
Albedo	0.27	0.25	0.12	0.85	0.065	0.31	0.16	0.85	0.061	0.25	0.14	0.83	0.059
EFLUX	66	52	54	1402	-53	51	47	939	-31	95	79	1141	-16.09
QV2M	3.23×10^{-3}	2.9×10^{-3}	2.58×10^{-3}	1.9×10^{-2}	1.1×10^{-4}	2.79×10^{-3}	2.45×10^{-3}	1.74×10^{-2}	1.69×10^{-4}	3.99×10^{-3}	3.14×10^{-3}	1.98×10^{-2}	2.53×10^{-4}
PBLH	1070	946	578	3546	55	833	571	3521	55	1429	707	4736	61
SWGDN	465	373	150	772	10.32	411	169	868	9.49	610	213	1030	15.81
RH	0.49	0.47	0.21	1	0.019	0.56	0.23	1	0.03	0.43	0.24	1	0.011